INTERNATIONAL JOURNAL FOR NUMERICAL METHODS IN ENGINEERING
Int. J. Numer. Meth. Engng 2004; **60**:2373–2398 (DOI: 10.1002/nme.1048)

On error estimator and *p*-adaptivity in the generalized finite element method

F. B. Barros[1,‡], S. P. B. Proença[2,*,†] and C. S. de Barcellos[3,§]

[1]*Department of Structural Engineering, School of Engineering of Federal University of Minas Gerais, Av. Contorno 842, Belo Horizonte, M.G., Brazil*
[2]*Department of Structural Engineering, São Carlos School of Engineering, University of São Paulo, Av. Trabalhador São-carlense, 400, São Carlos, S.P., CEP:13566-59, Brazil*
[3]*Pontifícia Universidade Católica, Belo Horizonte, M.G., Brazil*

SUMMARY

This paper addresses the issue of a *p*-adaptive version of the generalized finite element method (GFEM). The technique adopted here is the equilibrated element residual method, but presented under the GFEM approach, i.e., by taking into account the typical nodal enrichment scheme of the method. Such scheme consists of multiplying the partition of unity functions by a set of enrichment functions. These functions, in the case of the element residual method are monomials, and can be used to build the polynomial space, one degree higher than the one of the solution, in which the error functions is approximated. Global and local measures are defined and used as error estimator and indicators, respectively. The error indicators, calculated on the element patches that surrounds each node, are used to control a refinement procedure. Numerical examples in plane elasticity are presented, outlining in particular the effectivity index of the error estimator proposed. Finally, the *p*-adaptive procedure is described and its good performance is illustrated by the last numerical example. Copyright © 2004 John Wiley & Sons, Ltd.

KEY WORDS: finite element method; meshless methods; adaptivity; error estimation

1. INTRODUCTION

The generalized finite element method (GFEM) [1, 2], shares several features with the so-called meshless methods. In fact, the approximation functions used in the GFEM are associated with nodal points and the enrichment of the approximation spaces can be done at the nodes in the same fashion as in the meshless *hp*-cloud method [3]. On the other hand, the partition of unity [3, 4], used in the GFEM is provided by finite element shape functions. Therefore,

*Correspondence to: S. P. B. Proença, Department of Structural Engineering, São Carlos School of Engineering, University of São Paulo, Av. Trabalhador São-carlense, 400, São Carlos, S.P., Brazil, CEP:13566-59.
†E-mail: persival@sc.usp.br
‡E-mail: felicio@cadtec.dees.ufmg.br
§E-mail: clovis@pucminas.br

Received 21 November 2002
Revised 3 July 2003
Accepted 24 October 2003
Published online 11 June 2004

this method can also be understood as a non-conventional form of the finite element method. Incidentally, each cloud, i.e. the nodal region of influence, is built by a set of finite elements which surrounds each node as detailed in Reference [5]. Indeed, both interpretations of the GFEM are valid and give unique insights into the method.

The characteristic of nodal enrichment of the GFEM suggests an adaptive scheme to provide an automatic control. Moreover, as the polynomial functions fit very well with the GFEM enrichment strategy, a p-refinement can be taken into account. Therefore, the main objective of this paper is to present a p-adaptive strategy for the GFEM. The error measure used as an indicator to control the refinement scheme is evaluated by the element residual method, [6, 7]. Similarly, a global measure and also a local one associated with each element are proposed. These measures are found after solving a local Neumman boundary problem with residuals as data for each finite element. However, the local problems to be solved may not have a unique solution. The additional conditions necessary to guarantee uniqueness of the error problem can be achieved by following the residual equilibration scheme described in Reference [8] and adapted here to the GFEM. In spite of the error issue to be treated by elements, in coherence with GFEM the adaptive refinement must be conducted by nodal error values. Such nodal values are estimated here by a weighted average procedure of the element indicators.

The paper content is outlined on what follows. In Sections 2 and 3 the GFEM and its use in elasticity boundary value problems are briefly commented. Then a numerical application is presented in Section 4. The error estimator issue is addressed in Section 5. The implicit element residual method and its use in the GFEM is detailed in Section 5.1. In particular, local and global error estimators are proposed in Section 5.2 and an equilibrium strategy to the residual is presented in Section 5.3. Section 6 is devoted to the validation of the proposed estimators by controlling the effectivity indices computed in some classical elasticity problems. In Section 7 the p-adaptive scheme for nodal refinement is described. A numerical example is then shown in Section 8 to verify the efficiency of the adaptive proposition. Final considerations and conclusions are presented in Section 9.

2. THE GENERALIZED FINITE ELEMENT METHOD

According to Reference [2], the GFEM was proposed independently by:

- Babuška and coworkers, initially named as special finite element method [9], and later as the partition of unity finite element method [10, 11].
- Duarte and Oden, as a meshless formulation in the *hp*-cloud method [12, 13], and later as an hybrid approach with the FEM [14].

A similar philosophy is inserted in the works of Belytschko [15, 16], for discontinuous solutions and is called extended finite element method (XFEM).

In the GFEM [2], a set of partition of unity (PU) functions is employed to enforce interelement continuity, creating conforming approximations which are improved by a nodal enrichment strategy. This process of constructing approximation functions is described on what follows.

Let us consider, e.g. a conventional linear finite elements mesh, $\{\mathscr{K}_e\}_{e=1}^{NE}$ (being NE the number of elementos $\mathscr{K}_e$), defined by N nodes, $\{\mathbf{x}_j\}_{j=1}^{N}$, in a domain Ω, see Figure 1(a). The generic patch or cloud $\omega_j \in \Omega$ is obtained by the union of finite elements sharing the vertex

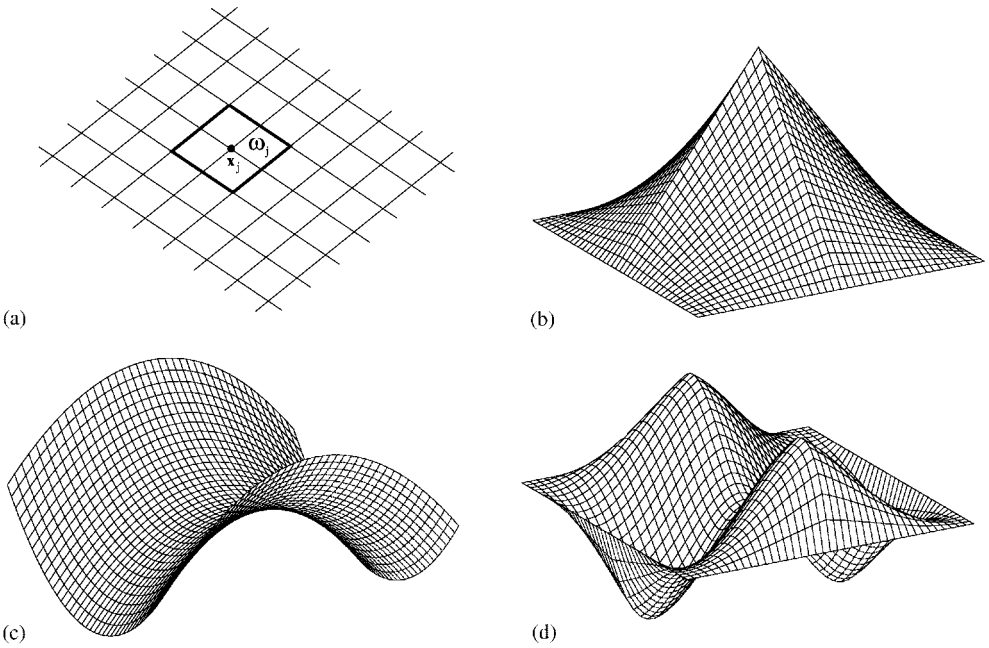

Figure 1. Enrichment scheme of the cloud ω_j: (a) cloud $\omega_j = \{\mathscr{K}_e \mid \mathscr{K}_e \supset \mathbf{x}_j\}$; (b) partition of unity function $\mathscr{N}_j$; (c) local approximation function L_{ji}; and (d) enriched shape function $\phi_{ji} = \mathscr{N}_j \times L_{ji}$.

node $\mathbf{x}_j$. The assemblage of the Lagrangian interpolating functions belonging to each element and associated with node $\mathbf{x}_j$ composes the function $\mathscr{N}_j$ defined over the support cloud ω_j. As $\sum_{j=1}^{N} \mathscr{N}_j = 1$ at every point $\mathbf{x}$ in the domain Ω, the set of functions $\{\mathscr{N}\}_{j=1}^{N}$ constitutes a partition of unity. Let us denote the following set of q linearly independent functions, defined at each cloud ω_j as

$$\mathscr{I}_j \stackrel{\text{def}}{=} \{L_{j1}(\mathbf{x}), L_{j2}(\mathbf{x}), \ldots, L_{jq}(\mathbf{x})\} \stackrel{\text{def}}{=} \{L_{ji}(\mathbf{x})\}_{i=1}^{q} \text{ with } L_{j1}(\mathbf{x}) = 1 \tag{1}$$

The generalized finite element shape functions associated with node $\mathbf{x}_j$ result from the enrichment, i. e. the multiplication, of the PU functions of the cloud ω_j by each of the components of (1):

$$\{\phi_{ji}\}_{i=1}^{q} = \mathscr{N}_j(\mathbf{x}) \times \{L_{ji}(\mathbf{x})\}_{i=1}^{q} \tag{2}$$

The linear combination leading to such shape functions can be understood by considering the representation depicted in Figure 1 for the case of approximations defined in $\mathbb{R}^2$. The enrichment scheme is obtained by multiplying a PU function (bi-linear) of C^0-type, Figure 1(b), and with compact support ω_j, by the function $L_{ji}(\mathbf{x})$, Figure 1(c), named in Reference [1] as a local approximation. The resulting shape function $\phi_{ji}(\mathbf{x})$, Figure 1(d), inherits characteristics of both functions, e.g. the compact support of the PU and the approximate character of the local function.

For instance, the generalized global approximation for the displacements, denoted as $\tilde{\mathbf{u}}(\mathbf{x})$, can then be described as a linear combination of the shape functions associated with each node:

$$\tilde{\mathbf{u}}(\mathbf{x}) = \sum_{j=1}^{N} \mathscr{N}_j(\mathbf{x}) \left\{ \mathbf{u}_j + \sum_{i=1}^{q} L_{ji}(\mathbf{x}) \mathbf{b}_{ji} \right\} \Rightarrow \tilde{\mathbf{u}} = \mathbf{\Phi}^{\mathrm{T}} \mathbf{U} \tag{3}$$

where $\mathbf{u}_j$ and $\mathbf{b}_{ji}$ are nodal parameters associated with the components $\mathscr{N}_j(\mathbf{x})$ and $\mathscr{N}_j(\mathbf{x}) \cdot L_{ji}(\mathbf{x})$ of the shape functions, respectively. The continuity of this function is granted by the compact support of the PU ($\mathscr{N}_j(\mathbf{x}) = 0$ on the boundary of ω_j), which also allows the pasting together of different local functions ($L_{ji}(\mathbf{x})$) specially chosen to each cloud ω_j.

3. THE MODEL BOUNDARY VALUE PROBLEM - FUNDAMENTAL EQUATIONS

Let us consider the linear elasticity boundary value problem, BVP, defined in the domain $\Omega \in \mathbb{R}^2$ with a reference system x-y.

$$\text{Find } \mathbf{u} \text{ such that: } \begin{cases} \nabla^{\mathrm{T}} \boldsymbol{\sigma}(\mathbf{u}) + \mathbf{b} = \mathbf{0} & \text{in } \Omega \\ \mathbf{u} = \hat{\mathbf{u}} & \text{on } \Gamma_{\mathrm{D}} \\ \mathbf{t}(\mathbf{u}) = \hat{\mathbf{t}} & \text{on } \Gamma_{\mathrm{N}} \end{cases} \tag{4}$$

where

- $\mathbf{u}^{\mathrm{T}} \stackrel{\text{def}}{=} [u_x \ u_y]$ is the displacement vector;
- Γ_{D} and Γ_{N} denote complementary parts of the boundary $\partial\Omega$ where the Dirichlet and Neumman conditions are defined, respectively;
- $\boldsymbol{\sigma} = \mathbf{D}\boldsymbol{\varepsilon}$ is the stress tensor;
- $\boldsymbol{\varepsilon}$ is the strain tensor;
- $\mathbf{D}$ is the constitutive rigidity tensor;
- $\mathbf{b}$ is the vector of body forces;
- $\mathbf{t} = \boldsymbol{\sigma}\mathbf{n}$, is the traction vector;
- $\hat{\mathbf{u}}$ and $\hat{\mathbf{t}}$ are prescribed displacement and traction vectors;
- $\mathbf{n}$ is the unit normal on the boundary $\partial\Omega$.

Let $\mathscr{U}$ be the set of kinematically admissible functions and $\mathscr{V}$ denotes the space of admissible variations. Then, the corresponding variational form of this problem can be stated as

$$\text{Find } \mathbf{u} \in \mathscr{U} \text{ such that: } \mathscr{B}(\mathbf{u}, \mathbf{v}) = \mathscr{F}(\mathbf{v}) \quad \forall \mathbf{v} \in \mathscr{V} \tag{5}$$

where

- $\mathscr{U}$ and $\mathscr{V} \subset \mathscr{H}^1(\Omega)$.
- $\mathscr{H}^1(\Omega)$, the Hilbert space of degree 1, is the standard Sobolev space of square integrable functions whose first derivatives are square integrable as well, and that is defined on the domain Ω;

- the following variational operators are defined:

$$\mathscr{B}(\mathbf{u}, \mathbf{v}) = \int \int_{\Omega} \boldsymbol{\varepsilon}^{\mathrm{T}}(\mathbf{v}) \boldsymbol{\sigma}(\mathbf{u}) l_z \, \mathrm{d}x \, \mathrm{d}y$$

$$\mathscr{F}(\mathbf{v}) = \int \int_{\Omega} \mathbf{v}^{\mathrm{T}} \mathbf{b} l_z \, \mathrm{d}x \, \mathrm{d}y + \int_{\Gamma_{\mathrm{N}}} \mathbf{v}^{\mathrm{T}} \hat{\mathbf{t}} l_z \, \mathrm{d}s$$

- $\mathbf{v}^{\mathrm{T}} \stackrel{\mathrm{def}}{=} [v_x \;\; v_y]$ is the test function vector;
- $\boldsymbol{\varepsilon}(\mathbf{v})$ is obtained by the symmetric part of the gradient operation over $\mathbf{v}$;
- l_z is the dimension of the elastic body in z direction (thickness), assumed here as constant by simplification.

Let now $\mathscr{U}_h \subset \mathscr{U}$ be the subspace spanned by a set of kinematically admissible GFEM functions and $\mathscr{V}_h$ be the respective subspace of $\mathscr{V}$. Thus, the Galerkin approximation of (5) results from:

$$\text{Find } \tilde{\mathbf{u}} \in \mathscr{U}_h \text{ such that: } \mathscr{B}(\tilde{\mathbf{u}}, \tilde{\mathbf{v}}) = \mathscr{F}(\tilde{\mathbf{v}}) \;\; \forall \tilde{\mathbf{v}} \in \mathscr{V}_h \tag{6}$$

where $\tilde{\mathbf{u}}$ and $\tilde{\mathbf{v}}$ are obtained from expression (3) as

$$\tilde{\mathbf{u}}(\mathbf{x}) = \sum_{j=1}^{N} \mathscr{N}_j(\mathbf{x}) \left\{ \mathbf{u}_j + \sum_{i=1}^{q_j} L_{ji}(\mathbf{x}) \mathbf{b}_{ji} \right\} \Rightarrow \tilde{\mathbf{u}} = \boldsymbol{\Phi}^{\mathrm{T}} \mathbf{U} \tag{7}$$

$$\tilde{\mathbf{v}}(\mathbf{x}) = \sum_{j=1}^{N} \mathscr{N}_j(\mathbf{x}) \left\{ \mathbf{v}_j + \sum_{i=1}^{q_j} L_{ji}(\mathbf{x}) \mathbf{c}_{ji} \right\} \Rightarrow \tilde{\mathbf{v}} = \boldsymbol{\Phi}^{\mathrm{T}} \mathbf{V} \tag{8}$$

It must be outlined that the system of equations resulting from (6) can be positive semi-definite if the set of shape functions is linear dependent. This kind of system can be solved efficiently by the iterative procedure described in References [2, 17].

4. NUMERICAL EXAMPLE

Aiming to illustrate the enrichment strategy of the GFEM, the problem of a L-shaped plane elastic body, firstly studied under the GFEM approach in Reference [14], is used. The structure, with the geometry shown in Figure 2(a) and thickness l_z, is loaded by tractions that produce the following displacement field according to Reference [18]:

$$u_x = \frac{A_1}{2G} r^{\lambda_1} \{ [\kappa - Q_1(\lambda_1 + 1)] \cos \lambda_1 \theta - \lambda_1 \cos(\lambda_1 - 2)\theta \} \tag{9}$$

$$u_y = \frac{A_1}{2G} r^{\lambda_1} \{ [\kappa + Q_1(\lambda_1 + 1)] \sin \lambda_1 \theta + \lambda_1 \sin(\lambda_1 - 2)\theta \} \tag{10}$$

in which

- u_x and u_y are the displacements components at directions x and y, respectively;
- A_1 is an arbitrary constant;

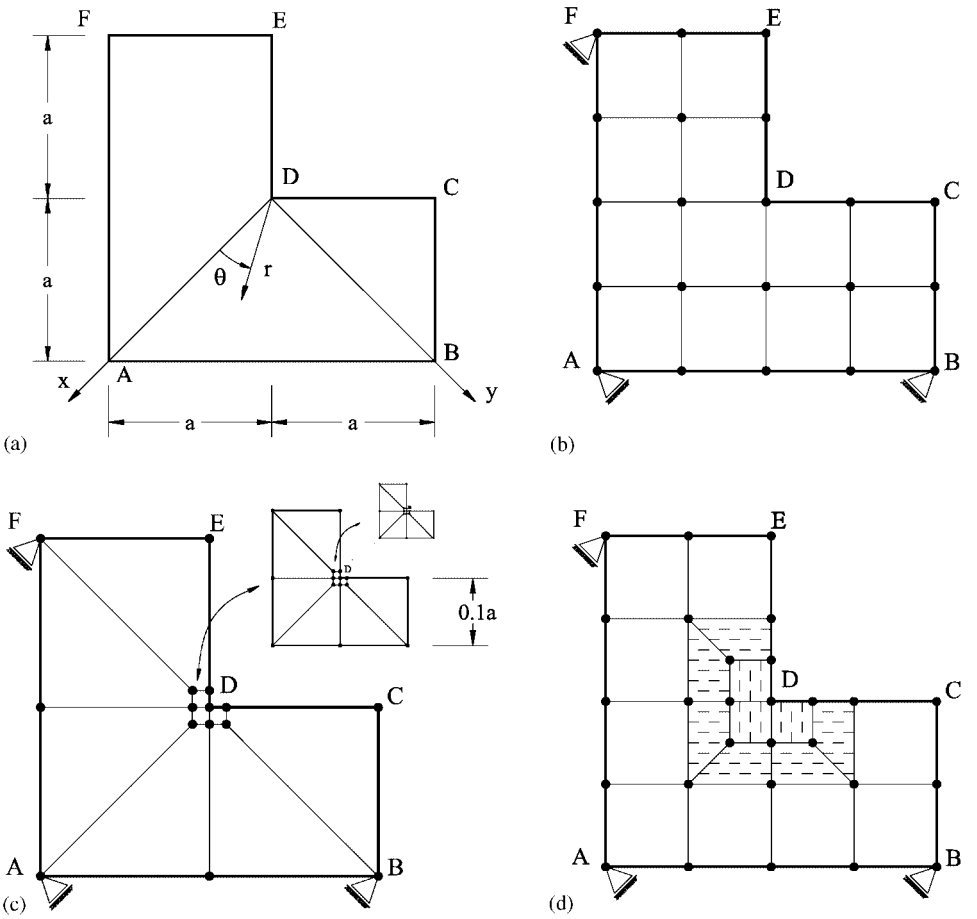

Figure 2. L-shaped domain: (a) geometry; (b) mesh used to p-refinement (p-GFEM); (c) strongly graded mesh (hp-GFEM); (d) mesh used to $psol$-GFEM$_1$ and $psol$-GFEM$_2$.

- $\lambda_1 = 0.544\,483\,737$ and $Q_1 = 0.543\,075\,579$ are constants determined so that solutions (9) and (10) satisfy the equilibrium and the free boundary conditions on the sides CD and DE;
- the plane strain condition is considered with $\kappa = 3 - 4\nu$;
- $G = E/2(1+\nu)$ and E is the Young modulus (in this example the solution is calculated as a function of E);
- the Poisson ratio $\nu = 0.3$.

The stress components which are used to load the body along the sides AB, BC, EF and FA are:

$$\sigma_x = A_1\lambda_1 r^{\lambda_1-1}\{[2 - Q_1(\lambda_1+1)]\cos(\lambda_1-1)\theta - (\lambda_1-1)\cos(\lambda_1-3)\theta\} \tag{11}$$

$$\sigma_y = A_1\lambda_1 r^{\lambda_1-1}\{[2+Q_1(\lambda_1+1)]\cos(\lambda_1-1)\theta+(\lambda_1-1)\cos(\lambda_1-3)\theta\} \tag{12}$$

$$\tau_{xy} = A_1\lambda_1 r^{\lambda_1-1}\{(\lambda_1-1)\sin(\lambda_1-3)\theta+Q_1(\lambda_1+1)\sin(\lambda_1-1)\theta\} \tag{13}$$

Since the loading satisfies the equilibrium, only rigid body constraints need to be applied as it is shown in Figure 2.

In this example, the stress components are singular on the point D which corresponds to the position $r = 0.0$. In order to evaluate the influence of such singularity over the rate convergence of GFEM approximation, four different sequences of refinements are performed:

p-GFEM: a bi-linear PU, provided by the finite element shape functions, is built over the mesh of the Figure 2(b). Then a uniform polynomial enrichment is done, for the degree p ranging from 1 to 8. For each degree p, the set of functions (1) is constructed by the monomials necessary to obtain the corresponding degree of the approximation. Details of this strategy are presented in the next section, where the space of the polynomials shape functions is defined.

hp-GFEM: in Figure 2(c) a sequence of strongly graded mesh, with the size of the elements decreasing in geometric progression toward to point D, is used to build a bi-linear PU. The distribution enrichment degree p varies linearly from the node D ($p = 1$) to the boundaries ABC and EFA ($p = p_{\max}$). This means that each cloud ω_j is enriched with a specific set of monomials $\mathscr{I}_j$ which corresponds to the p degree assigned by its position.

psol-GFEM$_1$: the mesh of the Figure 2(d) is used to build a bi-linear PU. The enrichment of the approximation is performed by a special set of functions $\mathscr{I}_j$, which is obtained by including the solution of the problem in the early mentioned set of monomials, i.e.:

$$1-\frac{u_x(\mathbf{x})}{u_x(\mathbf{x}_j)} \quad \text{for the approximation of the displacement } u_x \tag{14}$$

$$1-\frac{u_y(\mathbf{x})}{u_y(\mathbf{x}_j)} \quad \text{for the approximation of the displacement } u_y \tag{15}$$

Note that the above expressions are normalized to minimize the round-off errors of the results [3], and becomes null at $x = x_j$ to allow the direct imposition of the essential boundary conditions. The sequence of approximations is obtained by a uniform p-refinement performed for all the clouds, ranging from $p = 1$ to 5. At each approximation, expressions (14) and (15) multiply the PU functions of the clouds that contain the elements hatched by the vertical dashed lines in Figure 2(d).

psol-GFEM$_2$: the same procedure of *psol*-GFEM$_1$ is used, except from the fact that the solution enrichment, with expressions (14) and (15), is performed for all the clouds.

For each sequence of refinements described above, the energy norm defined as

$$\|\tilde{\mathbf{u}}\|_{\mathscr{U}(\Omega)} \stackrel{\text{def}}{=} [\mathscr{B}(\tilde{\mathbf{u}},\tilde{\mathbf{u}})]^{1/2} \tag{16}$$

was computed and presented in Tables I and II. Because the displacement field is known, expressions (9) and (10), the exact energy norm can be calculated as $2.8825490[A_1^2 a^{2\lambda} l_z/E]^{1/2}$

Table I. Uniform p-refinement. Comparative results of the normalized energy norm given by FEM and GFEM analysis, the first one presented in Reference [18]. NDF means number of degrees of freedom.

p-FEM		p-GFEM	
NDF	$\left[\frac{\|\tilde{\mathbf{u}}\|^2_{\mathscr{U}(\Omega)}E}{A_1^2 a^{2\lambda} l_z}\right]^{1/2}$	NDF	$\left[\frac{\|\tilde{\mathbf{u}}\|^2_{\mathscr{U}(\Omega)}E}{A_1^2 a^{2\lambda} l_z}\right]^{1/2}$
39	2.7459827	39	2.7459827
103	2.8115681	123	2.8115681
167	2.8196208	207	2.8359994
255	2.8402228	333	2.8492349
367	2.8537151	501	2.8605256
503	2.8619213	711	2.8654549
663	2.8672439	963	2.8695395
847	2.8706381	1257	2.8723141

Table II. Comparative results of the normalized energy norm given by three types of GFEM enrichment. NDF means number of degrees of freedom.

hp-GFEM		$psol$-GFEM$_1$		$psol$-GFEM$_2$	
NDF	$\left[\frac{\|\tilde{\mathbf{u}}\|^2_{\mathscr{U}(\Omega)}E}{A_1^2 a^{2\lambda} l_z}\right]^{1/2}$	NDF	$\left[\frac{\|\tilde{\mathbf{u}}\|^2_{\mathscr{U}(\Omega)}E}{A_1^2 a^{2\lambda} l_z}\right]^{1/2}$	NDF	$\left[\frac{\|\tilde{\mathbf{u}}\|^2_{\mathscr{U}(\Omega)}E}{A_1^2 a^{2\lambda} l_z}\right]^{1/2}$
13	2.6466652	69	2.8522972	109	2.8825490
41	2.7513684	181	2.8815017	221	2.8825490
111	2.8631708	293	2.8823148	333	2.8825490
223	2.8799921	461	2.8825275	501	2.8825490
391	2.8821166	685	2.8825465	725	2.8825490

and used to compute the error in energy norm given by

$$\|\mathbf{e}\|_{\mathscr{U}} = \sqrt{\mathscr{B}(\mathbf{e},\mathbf{e})} = \sqrt{\mathscr{B}(\mathbf{u},\mathbf{u}) - \mathscr{B}(\tilde{\mathbf{u}},\tilde{\mathbf{u}})} \tag{17}$$

In this relation the orthogonality condition of the Galerkin approximation [4], is used and $\mathbf{e} = \mathbf{u} - \tilde{\mathbf{u}}$ is the error of the approximate solution $\tilde{\mathbf{u}}$. The behaviour of the GFEM analysis for the present problem can be observed in the Figure 3, where the logarithm of the error in energy norm is plotted versus the logarithm of the number of degrees of freedom (NDF). The present problem is also solved in Reference [18], with the mesh of the Figure 2(b) and a sequence of p-uniform refinements for the hierarchic FEM. The results of such analysis, named here p-FEM, are reproduced in Table I and Figure 3 and are compared with the GFEM analysis.

The low rate of convergence of the p-FEM can be explained by the kind of solution of the problem analysed which is not smooth. A similar behaviour is reproduced by the p-GFEM. Such similarity was already expected because, for a regular mesh, the approximate space spanned by the FEM hierarchic shape functions is equivalent to the space built with the monomial enrichment of the PU functions used in the p-GFEM. The exponential rate

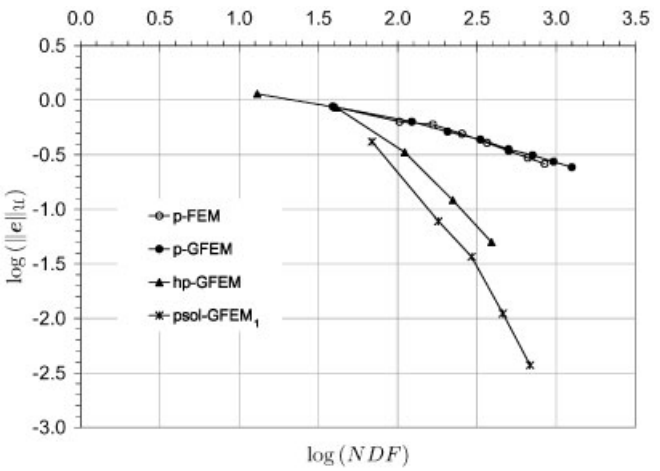

Figure 3. Relationship between error in energy norm and number of degrees of freedom (NDF) for different kinds of refinement strategies.

of convergence is recovery by the *hp*-GFEM analysis. This is accomplished thanks to the sequence of meshes and corresponding polynomials degrees properly selected to each cloud. An equivalent convergence could be achieved with the hierarchic version of FEM and the same sequence of geometric meshes. However, the enrichment strategy avoiding the side and internal nodes of the standard hierarchic FEM is an important advantage of the GFEM analysis. Therefore, the task of building conform approximations becomes quite straightforward. A non-uniform h and p approximation can be easily used without concerns about the connectivity of the mesh [2], which is a very interesting characteristic in an adaptive approach. The possibility to take advantage of such a enhancement motivated the present work, leading to the error measure and refinement strategy described in the next sections.

From the Table II and Figure 3 it is possible to see that the better results are obtained with the *psol*-GFEM$_1$ and *psol*-GFEM$_2$. This is not a surprise since the exact solution is used to enrich the PU functions. In the case of *psol*-GFEM$_2$, the results are not plotted because of scale reasons, since the error is too small to be drawn. When the enrichment is performed in the whole domain, the approximate solution can be considered as the exact one for any p-degree. There are, of course, some errors due to the lack of precision of the applied boundary conditions, numerical integration and round off errors. On the other hand, for *psol*-GFEM$_1$ analysis, the behaviour of the convergence rate is similar to the one of the *hp*-GFEM. The reason for this fact may be found at the set of elements that in the Figure 2(d) are marked with horizontal dashed lines. These elements have their four nodes enriched with monomials but only two of them, the closest ones of the singular point, have the solution enrichment. In this region the approximation is not able to exactly reproduce the solution function because the enrichment is not complete for all the nodes of the elements. In Reference [19], such a region is named blending sub-domain and it is shown that its presence can negatively affect the accuracy and the rate of convergence of the method. Two strategies aiming to overcome this problem are described, the first based on the Hu–Washizu variational principle and the other one through a enhanced strain field.

In spite of these facts, it is important to point out other advantages of the GFEM, such as the possibility of improving the approximation with non-polynomial functions enrichment. Several works have already been published in this context as References [20–22] and in the XFEM approach it can be mentioned the contributions of [15, 16, 23]. Another interesting characteristic is related to the presence of distorted elements, Figure 2(d). Differently from the standard FEM, in GFEM the cloud-based hierarchic forms build the approximation directly in the global coordinate system, retaining the accuracy of the spectral order p and providing the completeness of the shape functions [14].

5. ERROR ESTIMATOR

The p-adaptive procedure described in Section 7 is tailored to the nodal enrichment approach of the GFEM. In short, each node associated with a cloud that presents the largest local errors is selected for polynomial refinement so that the accuracy can be improved in the next solution of iterative step. The element residual method (ERM) introduced in References [24, 25] and extensively studied in References [26–29], can conveniently estimate the energy norm of the local approximation of the error at the element level. However, to achieve a measure that can be used as an error indicator in the context of the GFEM, it is necessary to define a local error associated with each cloud. This is obtained by considering such measure as an average value of the approximation error estimated on the boundaries and in the interior of the elements that share each vertex node. This is the subject of the next subsections, i.e. the adaptation of the ERM to the GFEM approach. Still in the GFEM context, a different strategy is used in Reference [17] to estimate the error energy norm. In such work a recovery GFEM solution is constructed and it is used to govern a h-adaptive refinement.

5.1. Implicit element residual method

The ERM described here is based on the formulation presented in References [6, 7]. In the following discussion, such method is adapted to the GFEM approach taking into account the enriched approximation functions of the Section 2. Two important issues can be pointed out. The first one, discussed in Section 5.2, refers to the indicator error which should be defined at the cloud level instead of the element level as it is usual. The other one is related to the strategy to equilibrate the residual and it is described in Section 5.3.

Firstly, let us consider the solution $\mathbf{u}_p$ of problem (6) and given by expression (7). The index p denotes the polynomial character of the resulting approximation. Accordingly, in the case of $\Omega \in \mathbb{R}^2$, the set of linearly independent functions stated in (1) is represented as

$$\mathscr{I}_j^p \stackrel{\text{def}}{=} \{1, p_{j1}^{rs}(\mathbf{x}), p_{j2}^{rs}(\mathbf{x}), \ldots, p_{jq}^{rs}(\mathbf{x})\} \tag{18}$$

where, p_{ji} is a typical monomial of degree $r(i)$ in x and degree $s(i)$ in y, associated with the cloud ω_j, and defined by

$$p_{ji}^{rs}(\mathbf{x}) = \left(\frac{x - x_j}{h_j^x}\right)^{r(i)} \left(\frac{y - y_j}{h_j^y}\right)^{s(i)} \tag{19}$$

being h_j^x and h_j^y characteristic sizes of the cloud in x and y directions, respectively.

The space spanned by the shape functions and resulting from the product of the PU functions by the set of polynomials $\mathscr{I}_j^p$ is denoted as $\mathscr{X}_p$. The error of an approximation $\mathbf{u}_p$ belonging to such space can be defined as

$$\mathbf{e}_p = \mathbf{u} - \mathbf{u}_p \tag{20}$$

where $\mathbf{u}$ refers to the exact solution of the BVP. By replacing, $\mathbf{u} = \mathbf{e}_p + \mathbf{u}_p$ into (4), a new problem to the error function $\mathbf{e}_p$ can be stated as

$$\begin{aligned} &\text{Find } \mathbf{e}_p \text{ such as} \\ &\nabla^{\mathrm{T}}\boldsymbol{\sigma}(\mathbf{e}_p) + \mathbf{r}_\Omega(\mathbf{u}_p) = \mathbf{0} && \text{in } \Omega \\ &\mathbf{e}_p = \mathbf{0} && \text{on } \Gamma_{\mathrm{D}} \\ &\mathbf{t}(\mathbf{e}_p) = \mathbf{r}_\Gamma(\mathbf{u}_p) && \text{on } \Gamma_{\mathrm{N}} \end{aligned} \tag{21}$$

where the residual functions are defined in the domain and on the boundary of the body, respectively, as

$$\begin{aligned} \mathbf{r}_\Omega(\mathbf{u}_p) &= \nabla^{\mathrm{T}}\boldsymbol{\sigma}(\mathbf{u}_p) + \mathbf{b} && \text{in } \Omega \\ \mathbf{r}_\Gamma(\mathbf{u}_p) &= \hat{\mathbf{t}} - \mathbf{t}(\mathbf{u}_p) && \text{on } \Gamma_{\mathrm{N}} \end{aligned} \tag{22}$$

Here, it is assumed, without loss of generality, that the essential boundary conditions are exactly satisfied. One important remark refers to the smoothness of the error function that is not the same as the one of $\mathbf{u}$. Actually, the term $\nabla^{\mathrm{T}}\boldsymbol{\sigma}(\mathbf{e}_p)$ may be not defined in some regions such as the common boundaries between neighbouring elements. Therefore, problem (21) must be understood by considering its weak form as it is done later in this subsection.

Before writing the weak form, it is interesting to formulate problem (21) locally for each element $\mathscr{K}$ that builds some cloud, aiming to achieve local measures of the error. In this case, a new natural boundary condition must be imposed at the edges between $\mathscr{K}$ and its neighbouring elements, $(\partial\mathscr{K}\backslash\partial\Omega)$. Such a condition defines the correspondent error in the tractions $\mathbf{t}(\mathbf{u}_p)$. However, as the true traction is unknown, it is replaced by $\langle\mathbf{t}(\mathbf{u}_p)\rangle_a = 1/2\{\mathbf{t}(\mathbf{u}_p) + \mathbf{t}(\mathbf{u}_p^*)\}$, that denotes the average of the approximate tractions evaluated on $\partial\mathscr{K}\backslash\partial\Omega$ from the values $\mathbf{t}(\mathbf{u}_p)$ defined at $\mathscr{K}$ and its neighbouring elements $(\mathbf{t}(\mathbf{u}_p^*))$. Finally, the BVP associated with the local error can be described as follows:

$$\begin{aligned} &\text{In the element } \mathscr{K}, \text{ find } \mathbf{e}_p \text{ such as:} \\ &\nabla^{\mathrm{T}}\boldsymbol{\sigma}(\mathbf{e}_p) + \mathbf{r}_\Omega(\mathbf{u}_p) = \mathbf{0} && \text{in } \mathscr{K} \\ &\mathbf{e}_p = \mathbf{0} && \text{on } \mathscr{K} \cap \Gamma_{\mathrm{D}} \\ &\mathbf{t}(\mathbf{e}_p) = \mathbf{r}_\Gamma(\mathbf{u}_p) && \text{on } \mathscr{K} \cap \Gamma_{\mathrm{N}} \\ &\boldsymbol{\sigma}(\mathbf{e}_p)\mathbf{n} = \langle\mathbf{t}(\mathbf{u}_p)\rangle_a - \mathbf{t}(\mathbf{u}_p) && \text{on } \partial\mathscr{K}\backslash\partial\Omega \end{aligned} \tag{23}$$

Note that the above problem becomes a Neumman or mixed problem as the element $\mathscr{K}$ lies in the interior of the domain or intersects the body boundary.

Now, the weak solution can be searched for. In Reference [6], the Galerkin approximate form of this problem can be accomplished by taking the bubble-like function space. Here, an analogous space can be build by using the set of shape functions of the GFEM. In this case, a 'cloud-bubble' character of each function is acquired by considering its respective compact support, by following the concept illustrated in Figure 1. Taking the previous considerations into account the function space, named $\mathscr{X}^0_{p+1}$, can be defined by using the GFEM shape functions analogously as in Reference [16]:

$$\mathscr{X}^0_{p+1}(\mathscr{K}) = \{\mathbf{v}^0_{p+1} \in \mathscr{X}_{p+1}(\mathscr{K});\ \ \Pi_p(\mathbf{v}^0_{p+1}) = 0;\ \ \mathbf{v}^0_{p+1} = 0 \text{ on } \partial\mathscr{K} \cap \Gamma_D\} \tag{24}$$

where $\Pi_p : \mathscr{H}^r(\mathscr{K}) \to \mathscr{X}_p(\mathscr{K})$ is the local interpolation operator and r is defined according to Reference [6]. Presently, instead of $\mathscr{H}^r(\mathscr{K})$, the polynomial space $\mathscr{X}_{p+1}(\mathscr{K}) \subset \mathscr{H}^r(\mathscr{K})$ is used. The motivation for this choice is the assumption that the most important part of the error can be represented by the monomial terms with one degree higher than the one of the approximate solution space $\mathscr{X}_p$ of $\mathbf{u}_p$. This assumption produces the space $\mathscr{X}^0_{p+1}(\mathscr{K})$ (the kernel of the operator Π_p) spanned by the functions $\mathbf{v}^0_{p+1}$ that belong to the space $\mathscr{X}_{p+1}(\mathscr{K})$ and vanish on the boundary $\partial\mathscr{K} \cap \Gamma_D$. Summarizing, what is being considering is the projection of the error onto the space $\mathscr{X}^0_{p+1}(\mathscr{K})$. Such space can be generated, in the case of the GFEM, by the shape functions (2) as it will be described on what follows.

A new boundary value problem, for each element $\mathscr{K}$ of a cloud, can now be written in the variational form as

$$\text{Find } \tilde{\mathbf{e}}_p \in \mathscr{X}^0_{p+1}(\mathscr{K}) \text{ such that:}$$

$$\begin{aligned}\mathscr{B}_{\mathscr{K}}(\tilde{\mathbf{e}}_p, \mathbf{v}^0_{p+1}) = &\int_{\partial\mathscr{K}\cap\Gamma_N} (\mathbf{v}^0_{p+1})^T \mathbf{r}_\Gamma(\mathbf{u}_p) l_z \, ds \\ &+ \int_{\partial\mathscr{K}\setminus\partial\Omega} (\mathbf{v}^0_{p+1})^T [\mathbf{t}(\mathbf{u}_p)] l_z \, ds + \int\int_{\mathscr{K}} (\mathbf{v}^0_{p+1})^T \mathbf{r}_\Omega(\mathbf{u}_p) l_z \, dx \, dy\end{aligned} \tag{25}$$

In the above formulation, $[\mathbf{t}(\mathbf{u}_p)] = 1/2\{\mathbf{t}(\mathbf{u}^*_p) - \mathbf{t}(\mathbf{u}_p)\}$, $\tilde{\mathbf{e}}_p$ is the Galerkin approximation of the error function $\mathbf{e}_p$, actually defining the error indicator function, and $\mathbf{v}^0_{p+1}$ is the test function of the problem. Both of them are described by the GFEM functions as

$$\tilde{\mathbf{e}}_p = (\mathbf{\Phi}^0_{p+1})^T \mathbf{I}^{\mathscr{K}} \tag{26}$$

$$\mathbf{v}^0_{p+1} = (\mathbf{\Phi}^0_{p+1})^T \mathbf{V}^0 \tag{27}$$

where the vector $\mathbf{\Phi}^0_{p+1}$ is built by the set of shape functions of expression (2), after eliminating from the set $\{\phi^{p+1}_{ji}\}$ the terms of the subset $\{\phi^p_{ji}\}$. Here the functions L_{ij} are defined by the set of monomials (18) required to reproduce exactly complete polynomials of $p+1$ degree, in the case of the set $\{\phi^{p+1}_{ji}\}$, and p in the case of the set $\{\phi^p_{ji}\}$. $\mathbf{I}^{\mathscr{K}}$ and $\mathbf{V}^0$ are nodal parameter vectors associated to each shape function of the set $\mathscr{X}^0_{p+1}(\mathscr{K})$. The vector $\mathbf{I}^{\mathscr{K}}$, in particular, is named the vector of error indicators.

Nevertheless, the last integral in problem (25) requires that the second derivative of the displacement approximation function must be defined everywhere in the discretized domain. In general this is not the case for the solution found for problem (6), so in Reference [30] it is suggested a different representation that can be obtained after replacing the residual definitions (22) in (25) and rewriting $[\mathbf{t}(\mathbf{u}_p)]$ as it was defined:

$$\begin{aligned}\mathscr{B}_{\mathscr{K}}(\tilde{\mathbf{e}}_p, \mathbf{v}^0_{p+1}) = &\int_{\partial\mathscr{K}\cap\Gamma_N} (\mathbf{v}^0_{p+1})^T[\hat{\mathbf{t}} - \mathbf{t}(\mathbf{u}_p)] l_z \, ds \\ &+ \int_{\partial\mathscr{K}\setminus\partial\Omega} (\mathbf{v}^0_{p+1})^T 1/2[\mathbf{t}(\mathbf{u}^*_p) - \mathbf{t}(\mathbf{u}_p)] l_z \, ds \\ &+ \int\int_{\mathscr{K}} (\mathbf{v}^0_{p+1})^T[\nabla^T\boldsymbol{\sigma}(\mathbf{u}_p) + \mathbf{b}] l_z \, dx \, dy \end{aligned} \tag{28}$$

The term with $\boldsymbol{\sigma}(\mathbf{u}_p)$ can be integrated by parts which gives, after applying the divergence theorem:

$$\begin{aligned}\mathscr{B}_{\mathscr{K}}(\tilde{\mathbf{e}}_p, \mathbf{v}^0_{p+1}) = &\int_{\partial\mathscr{K}\cap\Gamma_N} (\mathbf{v}^0_{p+1})^T[\hat{\mathbf{t}} - \mathbf{t}(\mathbf{u}_p)] l_z \, ds \\ &+ \int_{\partial\mathscr{K}\setminus\partial\Omega} (\mathbf{v}^0_{p+1})^T 1/2[\mathbf{t}(\mathbf{u}^*_p) - \mathbf{t}(\mathbf{u}_p)] l_z \, ds + \int\int_{\mathscr{K}} (\mathbf{v}^0_{p+1})^T \mathbf{b} l_z \, dx \, dy + \\ &- \int\int_{\mathscr{K}} (\boldsymbol{\varepsilon}^T(\mathbf{v}^0_{p+1})\boldsymbol{\sigma}(\mathbf{u}_p) l_z \, dx \, dy + \int_{\partial\mathscr{K}} (\mathbf{v}^0_{p+1})^T \mathbf{t}(\mathbf{u}_p) l_z \, ds \end{aligned} \tag{29}$$

Finally, taking into consideration the definitions of the operators $\mathscr{B}(\bullet, \bullet)$ and $\langle\bullet\rangle_a$ a new description to the Galerkin approximation of the error problem can be given by

$$\begin{aligned}&\text{Find } \tilde{\mathbf{e}}_p \in \mathscr{X}^0_{p+1}(\mathscr{K}) \text{ such that:} \\ &\quad \mathscr{B}_{\mathscr{K}}(\mathbf{e}_p, \mathbf{v}^0_{p+1}) = \mathscr{L}_{\mathscr{K}}(\mathbf{v}^0_{p+1}) \quad \forall \mathbf{v}^0_{p+1} \in \mathscr{X}^0_{p+1}(\mathscr{K})\end{aligned} \tag{30}$$

where

$$\begin{aligned}\mathscr{L}_{\mathscr{K}}(\mathbf{v}^0_{p+1}) \stackrel{\text{def}}{=} &\int\int_{\mathscr{K}} (\mathbf{v}^0_{p+1})^T \mathbf{b} l_z \, dx \, dy - \mathscr{B}_{\mathscr{K}}(\mathbf{u}_p, \mathbf{v}^0_{p+1}) \\ &+ \int_{\partial\mathscr{K}\cap\Gamma_N} (\mathbf{v}^0_{p+1})^T \hat{\mathbf{t}} l_z \, ds + \int_{\partial\mathscr{K}\setminus\partial\Omega} (\mathbf{v}^0_{p+1})^T \langle\mathbf{t}(\mathbf{u}_p)\rangle_a l_z \, ds \end{aligned} \tag{31}$$

The above problem leads to the following system of equations, at each element $\mathscr{K}$:

$$\mathbf{K}^{\mathscr{K}}_{\text{er}} \mathbf{I}^{\mathscr{K}} = \mathbf{R}^{\mathscr{K}} \tag{32}$$

where

$$\mathbf{K}_{\mathrm{er}}^{\mathscr{K}} = \int\int_{\mathscr{K}} (\mathbf{B}_{p+1}^{0})^{\mathrm{T}} \mathbf{C} \mathbf{B}_{p+1}^{0} l_z \, \mathrm{d}x \, \mathrm{d}y \tag{33}$$

$$\mathbf{R}^{\mathscr{K}} = \int\int_{\mathscr{K}} (\mathbf{\Phi}_{p+1}^{0}) \mathbf{b} l_z \, \mathrm{d}x \, \mathrm{d}y - \mathbf{K}^{\mathscr{K}} \mathbf{U} + \int_{\partial\mathscr{K} \cap \Gamma_{\mathrm{N}}} (\mathbf{\Phi}_{p+1}^{0}) \hat{\mathbf{t}} l_z \, \mathrm{d}s + \int_{\partial\mathscr{K} \setminus \partial\Omega} (\mathbf{\Phi}_{p+1}^{0}) \langle \mathbf{t}(\mathbf{u}_p) \rangle_a l_z \, \mathrm{d}s \tag{34}$$

$$\mathbf{K}^{\mathscr{K}} = \int\int_{\mathscr{K}} (\mathbf{B}_p)^{\mathrm{T}} \mathbf{C} \mathbf{B}_p l_z \, \mathrm{d}x \, \mathrm{d}y \tag{35}$$

$$\mathbf{B}_{p+1}^{0} = \mathbf{L}(\mathbf{\Phi}_{p+1}^{0})^{\mathrm{T}} \tag{36}$$

$$\mathbf{B}_p = \mathbf{L}(\mathbf{\Phi}_p)^{\mathrm{T}} \tag{37}$$

where $\mathbf{L}$ is the gradient operator of the strain field.

5.2. Error measures

Local values of the energy norm of the function $\mathbf{e}_p$ obtained at each element can be estimated as

$$\tilde{\mathscr{E}}_{\mathscr{K}} \stackrel{\mathrm{def}}{=} \|\tilde{\mathbf{e}}_p\|_{\mathscr{U}(\mathscr{K})} = [\mathscr{B}_{\mathscr{K}}(\tilde{\mathbf{e}}_p, \tilde{\mathbf{e}}_p)]^{1/2} \tag{38}$$

where $\tilde{\mathscr{E}}_{\mathscr{K}}$ defines the error indicator for the element $\mathscr{K}$. The global error estimator is computed from the contribution of the local indicators:

$$\|\tilde{\mathbf{e}}_p\|_{\mathscr{U}} = \sqrt{\sum_{\mathscr{K} \in \Omega} \tilde{\mathscr{E}}_{\mathscr{K}}^2} \tag{39}$$

In the classical FEM the error indicators given by (38) can be used to define an adaptive procedure over the elements. However, in the GFEM, as it was already been pointed out at the beginning of Section 5, the p-refinement procedure is based on a nodal enrichment strategy. This approach motivates the introduction of a new error measure associated with the node (or the cloud) instead of that one attached to elements.

A simple way to define the error measure associated with each cloud ω_j is by the weighted average of the error indicators, given by (38), of the elements $\mathscr{K}$ contained in ω_j. Therefore, a nodal error indicator can be stated as:

$$\tilde{\mathscr{E}}_{\omega_j} \stackrel{\mathrm{def}}{=} \sum_{\mathscr{K} \in \omega_j} \frac{V_{\mathscr{K}} \|\tilde{\mathbf{e}}_p\|_{\mathscr{U}(\mathscr{K})}}{V_{\omega_j}} \tag{40}$$

where the volume of each element $\mathscr{V}_{\mathscr{K}}$ is employed as the weight and $V_{\omega_j} = \sum_{\mathscr{K} \in \omega_j} V_{\mathscr{K}}$ is the total volume of the cloud ω_j.

5.3. The equilibrated residual

Considering inner elements, BVP (30), corresponds to a Neumman problem as it involves only natural boundary conditions. As a consequence the problem to be approximated may not have a unique solution. This issue can be overcome building the approximate error with the functions of the space $\mathscr{X}^0_{p+1}(\mathscr{K})$ (24), that is a quotient space with the null space factored out. Even so, according to Reference [7], by using of the quotient space is not a guarantee of eliminating all spurious modes of the approximate error solution which arises from the locally defined boundary data. An efficient strategy do solve this problem can be achieved by requiring that the boundary data $\mathbf{r}_\Gamma$, $\mathbf{t}(\mathbf{u}_p)$ and $\langle \mathbf{t}(\mathbf{u}_p)\rangle_a$ be in equilibrium with the interior residual $\mathbf{r}_\Omega$. The accomplishment of this actually means to guarantee that the local error problem is well posed. Several strategies to impose such equilibrium have been proposed so far, among them References [8, 25, 31, 32].

In the present work, the method proposed in Reference [8] is used. The following discussion summarizes the fundamental steps of the procedure. The overview of the method is given here mainly with the purpose of indicating how this strategy can be applied in the GFEM approach.

The method consists of introducing a new traction distribution $\boldsymbol{\theta}^{\mathscr{K}}$ along the boundary of each element $\mathscr{K}$ in order to equilibrate the original set of boundary data. The equilibrium is then verified if the resulting force and moment are null for each element $\mathscr{K}$, i.e.

$$\int\int_{\mathscr{K}} \mathbf{r}_\Omega l_z \,\mathrm{d}x\,\mathrm{d}y + \int_{\partial\mathscr{K}\cap\Gamma_N} \mathbf{r}_\Gamma l_z \,\mathrm{d}s + \int_{\partial\mathscr{K}\setminus\partial\Omega} [\mathbf{t}(\mathbf{u}_p)] l_z \,\mathrm{d}s + \int_{\partial\mathscr{K}} \boldsymbol{\theta}^{\mathscr{K}} l_z \,\mathrm{d}s = \mathbf{0} \tag{41}$$

$$\begin{aligned}&\int\int_{\mathscr{K}} (\rho^y r^x_\Omega + \rho^x r^y_\Omega) l_z \,\mathrm{d}x\,\mathrm{d}y + \int_{\partial\mathscr{K}\cap\partial\Omega} (\rho^y r^x_\Gamma + \rho^x r^y_\Gamma) l_z \,\mathrm{d}s \\ &\quad + \int_{\partial\mathscr{K}\setminus\partial\Omega} (\rho^y [t^x(\mathbf{u}_p)] + \rho^x [t^y(\mathbf{u}_p)]) l_z \,\mathrm{d}s + \int_{\partial\mathscr{K}} (\rho^y \theta^{\mathscr{K}}_x + \rho^x \theta^{\mathscr{K}}_y) l_z \,\mathrm{d}s = \mathbf{0}\end{aligned} \tag{42}$$

where ρ^x and ρ^y are the distances between a generic point $\mathbf{x}$ in the element $\mathscr{K}$ and an arbitrary reference position $\mathbf{x}_0$ of Ω, measured in the reference directions x and y, respectively, Figure 4. In order to facilitate the determination of the traction distribution $\boldsymbol{\theta}^{\mathscr{K}}$, the concept of equivalent nodal forms must be used. According to Reference [8] and as it is shown in Reference [33], in the case of linear geometric mapping of the master element, Equations (41) and (42) can be replaced by the following nodal conditions:

$$\hat{\boldsymbol{\Theta}}^{\mathscr{K}}_j + \int\int_{\mathscr{K}} \boldsymbol{\phi}_j \mathbf{r}_\Omega l_z \,\mathrm{d}x\,\mathrm{d}y + \int_{\partial\mathscr{K}\cap\Gamma_N} \boldsymbol{\phi}_j \mathbf{r}_\Gamma l_z \,\mathrm{d}s + \int_{\partial\mathscr{K}\setminus\partial\Omega} \boldsymbol{\phi}_j [\mathbf{t}(u_p)] l_z \,\mathrm{d}s = \mathbf{0} \tag{43}$$

in which the residual force associated with the nodes can be defined as

$$\hat{\boldsymbol{\Theta}}^{\mathscr{K}}_j \overset{\text{def}}{=} \int_{\partial\mathscr{K}} \hat{\boldsymbol{\phi}}_j \boldsymbol{\theta}^{\mathscr{K}} l_z \,\mathrm{d}s \tag{44}$$

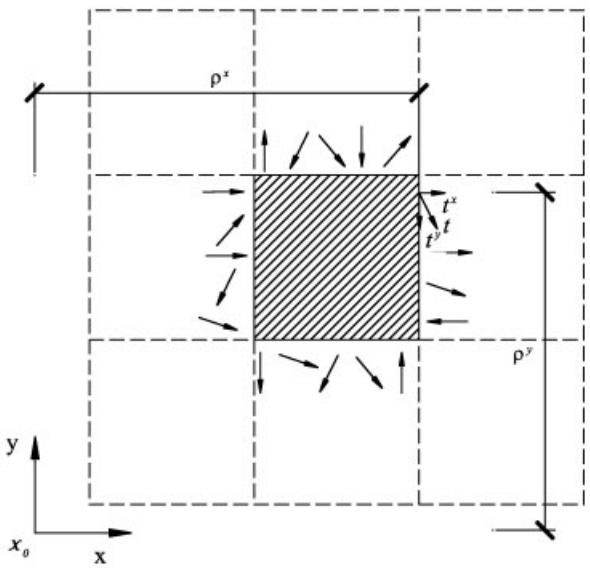

Figure 4. Scheme illustrating the distances ρ^x and ρ^y between the arbitrary point x_0 and the point where a boundary data (in the case $t(u_p)$) is applied over a generic finite element of a mesh.

and $\hat{\boldsymbol{\phi}}_j^{\mathrm{T}}$ is a sub-matrix with the shape functions associated with the node $\mathbf{x}$ in x and y directions:

$$\hat{\boldsymbol{\phi}}_j^{\mathrm{T}} = \begin{bmatrix} \mathscr{N}_j(\mathbf{x}) & 0 & p_{j1}^{rs}(\mathbf{x}) & \cdots & p_{jq}^{rs}(\mathbf{x}) & 0 \\ 0 & \mathscr{N}_j(\mathbf{x}) & 0 & p_{j1}^{rs}(\mathbf{x}) & \cdots & p_{jq}^{rs}(\mathbf{x}) \end{bmatrix} \tag{45}$$

Note that the shape functions, obtained by the expression (2), result from the multiplication of the PU functions by the set of polynomials given by (18).

In the particular case of the GFEM, it is important to point out that only the components of the residual forces associated with the PU (the first two columns of (45)) can affect the equilibrium. This means that only such components must be considered in Equation (43). In fact, the other components, associated with the enrichment functions are self-equilibrated and, as a consequence, they do not need to take part in this procedure. For this reason, the definition of $\hat{\boldsymbol{\phi}}_j$, (45), can be modified by using a more simple matrix:

$$\hat{\boldsymbol{\phi}}_j^{\mathrm{T}} = \begin{bmatrix} \mathscr{N}_j(\mathbf{x}) & 0 \\ 0 & \mathscr{N}_j(\mathbf{x}) \end{bmatrix} \tag{46}$$

The residual forces $\hat{\boldsymbol{\Theta}}_j^{\mathscr{K}}$ are then resolved into components applied to the sides of the elements. In Reference [8] this is performed by employing the Maxwell force diagrams in a very physical insight. The resulting discrete side forces are finally replaced back by statically equivalent traction distributions $\boldsymbol{\theta}^{\mathscr{K}}$ described by a linear interpolation of nodal parameters associated

with each edge of the element $\mathscr{K}$. Such parameters are obtained aiming to guarantee a unique interaction between adjacent elements.

6. NUMERICAL EXAMPLES

Two numerical examples are presented here in order to illustrate the application of the equilibrated element residual method with the GFEM approach. The main goal of this section is to show that good global and local error measures can be obtained if the error is approximated in the space $\mathscr{X}^0_{p+1}$, which is built by the enriched shape functions of the GFEM.

6.1. Linear bending problem

In Figure 5, a 2-D plane stress problem is represented, being the loading prescribed by the following expressions:

$$q_x = \frac{240y}{c} - 120 \tag{47}$$

$$q_y = \frac{120y}{L} - \frac{120y^2}{cL} \tag{48}$$

The exact analytical solution to this classical elasticity problem is given by [34]

$$u_x = \frac{1}{E}\left(\frac{120}{cL}x^2y - \frac{92}{cL}y^3 - \frac{60}{L}x^2 - \frac{240}{c}xy + \frac{138}{L}y^2 + 120x - \frac{46c}{L}y\right) \tag{49}$$

$$u_y = \frac{1}{E}\left(-\frac{40}{cL}x^3 - \frac{36}{cL}xy^2 + \frac{120}{c}x^2 + \frac{36}{L}xy + \frac{36}{c}y^2 + \frac{46c}{L}x - 36y\right) \tag{50}$$

where u_x and u_y are, respectively, the displacement in x and y directions.

The problem is solved by the conventional FEM, with a mesh of 10 quadrangular elements of linear approximation. Therefore, the approximate solution ($\mathbf{u}_p$) is linear. The objective of this example is to show the performance of the error measures defined in Section 5 by considering two kinds of cloud-bubble spaces, discussed on what follows. The enrichment strategy is not intended to be used here for the approximate solution but only for the REM. Numerical tests

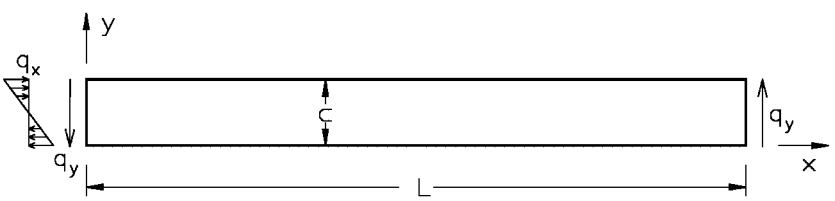

Figure 5. Geometry and loading. Young's modulus $E = 1 \times 10^7$, Poisson coefficient $v = 0.3$, thickness $t = 1.0$, $L = 100$ and $c = 10$.

in which the error measures are estimated for enriched solutions are presented in the next subsection.

According to Section 5.1, the space where the error functions should be projected ($\mathscr{X}_2^0$), is built by the following shape functions of the GFEM:

$$(\mathbf{\Phi}_2^0)_j^{\mathrm{T}} = \begin{bmatrix} \mathscr{N}_j(\mathbf{x}) \cdot \dfrac{x - x_j}{h_j} & 0 & \mathscr{N}_j(\mathbf{x}) \cdot \dfrac{y - y_j}{h_j} & 0 \\ 0 & \mathscr{N}_j(\mathbf{x}) \cdot \dfrac{x - x_j}{h_j} & 0 & \mathscr{N}_j(\mathbf{x}) \cdot \dfrac{y - y_j}{h_j} \end{bmatrix} \tag{51}$$

Moreover, aiming to improve the error measure it is possible to enlarge the space dimension ($\mathscr{X}_{2,3}^0$) by introducing new functions such as

$$(\mathbf{\Phi}_{2,3}^0)_j^{\mathrm{T}} = \begin{bmatrix} \mathscr{N}_j(\mathbf{x}) \cdot \dfrac{x - x_j}{h_j} & 0 & \mathscr{N}_j(\mathbf{x}) \cdot \dfrac{y - y_j}{h_j} & 0 \\ 0 & \mathscr{N}_j(\mathbf{x}) \cdot \dfrac{x - x_j}{h_j} & 0 & \mathscr{N}_j(\mathbf{x}) \cdot \dfrac{y - y_j}{h_j} \\ \mathscr{N}_j(\mathbf{x}) \cdot \left(\dfrac{x - x_j}{h_j}\right)^2 & 0 & \mathscr{N}_j(\mathbf{x}) \cdot \left(\dfrac{y - y_j}{h_j}\right)^2 & 0 \\ 0 & \mathscr{N}_j(\mathbf{x}) \cdot \left(\dfrac{x - x_j}{h_j}\right)^2 & 0 & \mathscr{N}_j(\mathbf{x}) \cdot \left(\dfrac{y - y_j}{h_j}\right)^2 \end{bmatrix} \tag{52}$$

This possibility is discussed in Reference [30] and it is named here as $\mathrm{REM}_{p+1,p+2}$ while the ($\mathscr{X}_2^0$) option is denoted as REM_{p+1}.

Since the exact solution for the displacements is known, the following exact error measures can be evaluated: one to each element, $\|\mathbf{e}_p\|_{\mathscr{U}(\mathscr{K})}$, and another one globally, $\|\mathbf{e}_p\|_{\mathscr{U}} = \sqrt{\sum_{\mathscr{K}\in\Omega} \|\mathbf{e}_p\|^2_{\mathscr{U}(\mathscr{K})}}$. Such measures and the approximate values given by (38) and (39) can then be employed to compute the effectivity indices, defined by

$$\eta_{\mathscr{K}} = \frac{\tilde{\mathscr{E}}_{\mathscr{K}}}{\|\mathbf{e}_p\|_{\mathscr{U}(\mathscr{K})}} \quad \text{local effectivity index} \tag{53}$$

$$\eta = \frac{\|\tilde{\mathbf{e}}_p\|_{\mathscr{U}}}{\|\mathbf{e}_p\|_{\mathscr{U}}} \quad \text{global effectivity index} \tag{54}$$

The effectivity indices can be employed to express the quality of the error measures of the linear solution of the FEM mesh adopted. The results are depicted in Figure 6 by considering the two possibilities for the error approximation. As a first conclusion it can be noted that the error is better approximated by the $\mathrm{REM}_{2,3}$, giving values closer to unity. However, the REM_2 performance is also quite reasonable. Actually, this possibility could be employed in a

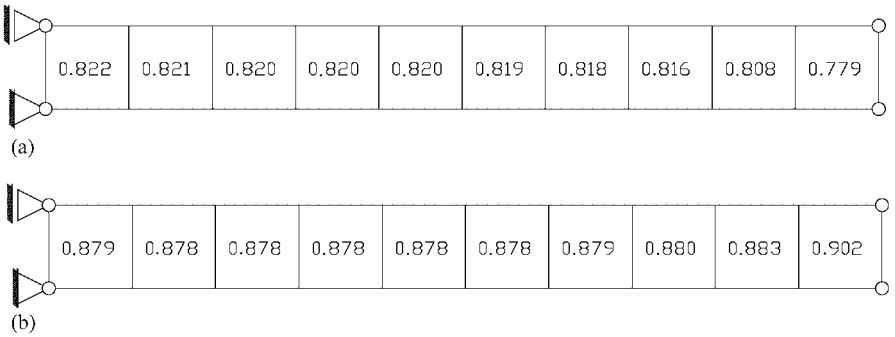

Figure 6. Local effectivity indices. Global relative error is 57.13% of the energy norm of the solution: (a) REM_2—global effectivity index $\eta = 0.820$; and (b) $REM_{2,3}$—global effectivity index $\eta = 0.878$.

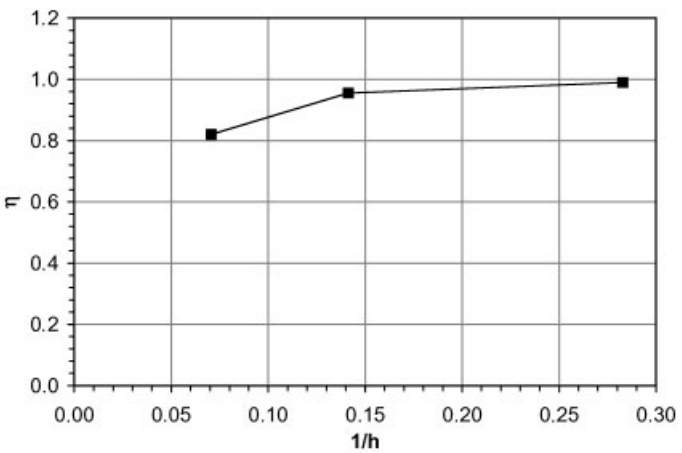

Figure 7. Global effectivity index (REM_2) for a nested sequence of meshes.

context where the costs associated with the increasing of space dimension plays an important rule (specially when the processing time is a key issue).

In face of the above discussion the analysis of the convergence of the error measure is performed only to the REM_2. With this objective a nested sequence of three meshes is used. The first of them is the original mesh of 10 elements, Figure 6, and the following two meshes are obtained by dividing each element of the previous mesh by four equal new elements. The points depicted in the Figure 7 correspond to the global effectivity index of each mesh. The results found indicate the increased performance of the error measure as the global effectivity index gets closer to unity as a consequence of the refinement process.

6.2. Circular hole in an infinite plate

Now the classical problem of a infinite plate with a circular hole, in plane strain state, subjected to unidirectional tension σ_∞ is considered, Figure 8(a). A FEM mesh with quadrangular

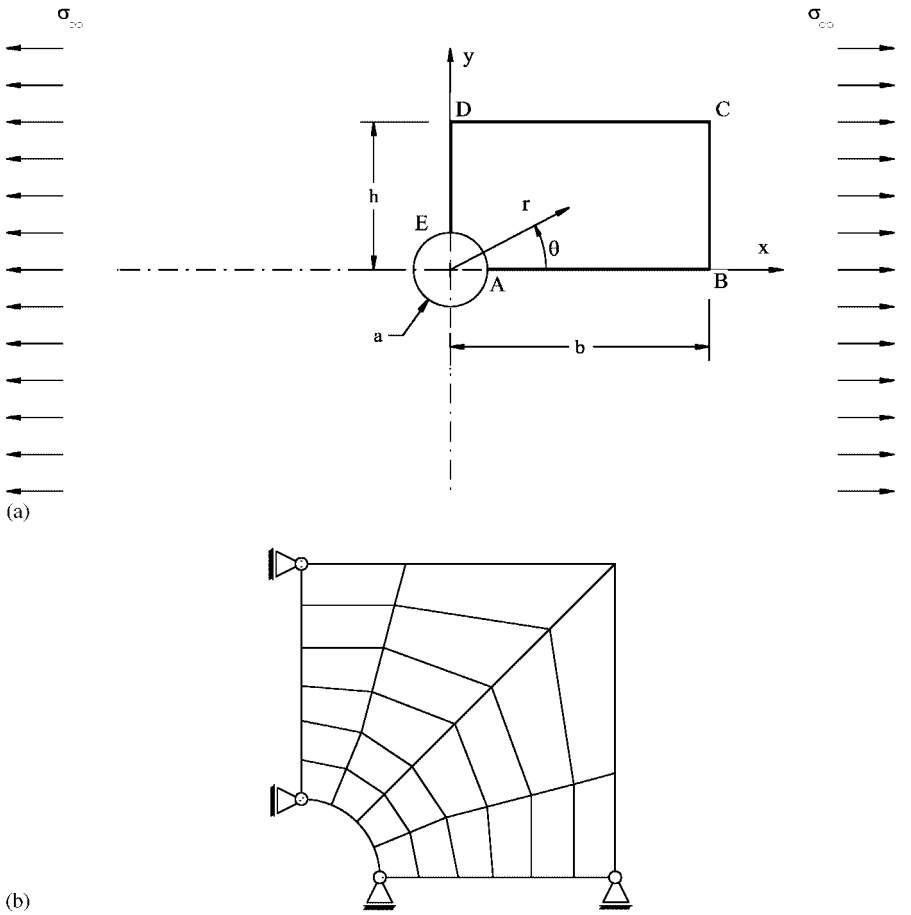

Figure 8. Circular hole in an infinite plate: (a) geometry and loading; and (b) finite element mesh.

elements of four nodes is shown in the Figure 8(b) and it is used to build the PU linear functions. The analysis is performed over the domain ABCDE. Symmetry conditions are imposed on the edges AB and DE. The following stress distribution obtained from the elastic solution [34], is imposed on the edges BC and CD:

$$\sigma_x = \sigma_\infty \left[1 - \frac{a^2}{r^2} \left(\frac{3}{2} \cos 2\theta + \cos 4\theta \right) + \frac{3a^4}{2r^4} \cos 4\theta \right] \tag{55}$$

$$\sigma_y = \sigma_\infty \left[-\frac{a^2}{r^2} \left(\frac{1}{2} \cos 2\theta - \cos 4\theta \right) - \frac{3a^4}{2r^4} \cos 4\theta \right] \tag{56}$$

$$\tau_{xy} = \sigma_\infty \left[-\frac{a^2}{r^2} \left(\frac{1}{2} \sin 2\theta + \cos 4\theta \right) + \frac{3a^4}{2r^4} \cos 4\theta \right] \tag{57}$$

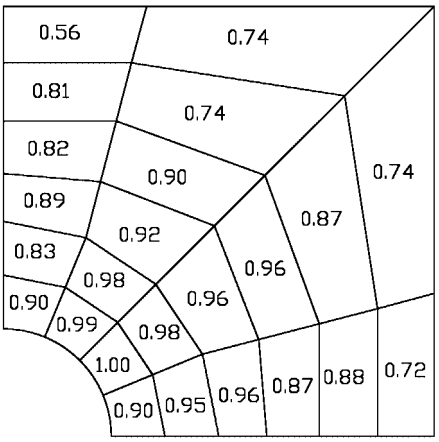

Figure 9. Local effectivity index $\eta_{\mathscr{K}}$ to each element $\mathscr{K}$. Global relative error is 9.7% of the energy norm of the solution.

The resulting displacement field is described by its components in the x and y directions:

$$u_x = \frac{\sigma_\infty a}{8G}\left\{\frac{r}{a}(\kappa+1)\cos\theta + \frac{2a}{r}[(1+\kappa)\cos\theta + \cos 3\theta] - \frac{2a^3}{r^3}\cos 3\theta\right\} \tag{58}$$

$$u_y = \frac{\sigma_\infty a}{8G}\left\{\frac{r}{a}(\kappa-3)\sin\theta + \frac{2a}{r}[(1-\kappa)\sin\theta + \sin 3\theta] - \frac{2a^3}{r^3}\sin 3\theta\right\} \tag{59}$$

where $G = E/[2(1+\nu)]$ and $\kappa = 3-4\nu$. The adopted values to the parameters are the following: $a = 1.0$, $b = h = 4.0$, $E = 1.0$, $\nu = 0.3$ and $\sigma_\infty = 1.0$. In order to represent the curved boundary EA the linear blending function method, proposed in Reference [35], was adopted.

The local and the global estimations of the error are obtained after employing the REM_2 with the space of approximations built by the functions given in (51). By knowing the exact elastic solution, the same procedure described in Section 6.1 can be used to calculate the effectivity indices.

In Figure 9, the local values $\eta_{\mathscr{K}}$ to each element $\mathscr{K}$ are represented. One observes that for the great majority of the elements such values are close to the unity, indicating the good quality of the local error estimator. However, the same performance is not found in the elements far away from the hole, probably due to some interference of the fictitious imposed Dirichlet boundary conditions. Even so, the global effectivity index η is 0.939, very close to the unity, meaning a good accuracy of the global error measure.

7. THE ADAPTIVE PROCEDURE

The adaptive procedure used here, described by algorithm (1), is based on the strategies proposed in References [6, 30]. Essentially, the idea behind the procedure is to find an optimal p-approximation over a fixed mesh that produces, under an adopted tolerance, a uniform

distribution of the energy norm of the error. Such procedure is tailored here to the GFEM approach, by accounting for the nodal polynomial enrichment. So, in the place of the element indicators, the refinement is conducted by the nodal indicators $\tilde{\mathscr{E}}_{\omega_j}$ stated in (40).

In short, two kinds of error measures and three parameters are used in the refinement process:

- the relative global error indicator:

$$\tilde{\mathscr{E}}_{\%} \stackrel{\text{def}}{=} \frac{\|\tilde{\mathbf{e}}_p\|_{\mathscr{U}}}{\sqrt{(\|\mathbf{u}_p\|_{\mathscr{U}})^2 + (\|\tilde{\mathbf{e}}_p\|_{\mathscr{U}})^2}} \times 100\% \tag{60}$$

  where $\|\mathbf{u}_p\|_{\mathscr{U}}$ is the energy norm of the approximate solution and $\sqrt{(\|\mathbf{u}_p\|_{\mathscr{U}})^2 + (\|\tilde{\mathbf{e}}_p\|_{\mathscr{U}})^2}$ is an estimated value to the energy norm of the exact solution;
- the local error indicator $\tilde{\mathscr{E}}_{\omega_j}$, given by (40).
- the parameters: υ, $\text{TOL}_{\text{error}}$ and $p_{\max}$. Such parameters explained on what follows are very important to define the rate of convergence of the refinement and its stopping criterion.

Basically, in each step of the refinement process, the error indicator $\tilde{\mathscr{E}}_{\omega_j}$ of each cloud ω_j is compared to a local tolerance given by $\upsilon\tilde{\mathscr{E}}_{\max}$, where $\tilde{\mathscr{E}}_{\max}$ is the maximum value $\tilde{\mathscr{E}}_{\omega_j}$ found at the considered step. The parameter υ works then as the enrichment controller. The dimension of the space of the approximated solution is increased by enrichment of the PU functions associated with the clouds, where the local errors exceed a threshold ($\tilde{\mathscr{E}}_{\omega_j} > \upsilon\tilde{\mathscr{E}}_{\max}$). A new step is necessary if the relative global error $\tilde{\mathscr{E}}_{\%}$ is larger than an assumed tolerance $\text{TOL}_{\text{error}}$. The increasing of the polynomial degree of the approximation is locally limited by the parameter $p_{\max}$. If in all clouds where $\tilde{\mathscr{E}}_{\omega_j} > \upsilon\tilde{\mathscr{E}}_{\max}$ the polynomial degree have already exceeded the limit $p_{\max}$, then a smaller value to υ should be employed (for instance a value equivalent to 90% of the original one). The process diverges if $p_{\max}$ is the polynomial degree of all clouds. In this case it is impossible to reach a solution with a tolerance $\text{TOL}_{\text{error}}$ to the maximum polynomial degree adopted. This situation is controlled by the counter i_{end}.

8. NUMERICAL EXAMPLE

The problem of Section 6.2 is considered once again, aiming to illustrate the p-adaptive procedure discussed in the previous section. The starting mesh is the one represented in the Figure 8(b), where the approximation is linear ($p = 1$). According to algorithm (1) the numerical solution obtained is evaluated by the error estimators defined by the REM_{p+1}. The approximation is enriched by multiplying the PU functions by polynomials with one degree higher than that one employed at the previous adaptive step. It is very important to point out here the straightforward way by which the adaptive refinement is performed. Thanks to the enrichment strategy of the GFEM, no constraints over the approximation functions must be enforced, then implying in a very flexible adaptive procedure.

The degree of the cloud approximation is identified with the degree of the set of shape functions generated by the product of the PU functions and the polynomial multipliers (19). Those polynomials are added to the set $\mathscr{I}_j^p$ such that the resulting shape functions are equivalent

Algorithm 1: p-adaptive analysis.

Read the geometric and loading data.
Read υ, TOL_{error}, p_{max}, $i_p = 1$.
loop
  Assemble $\mathbf{K}$, $\mathbf{F}$
  Solves the system $\mathbf{KU} = \mathbf{F}$
  for $\mathscr{K} = 1$ to NEL **do**
    Assemble $\mathbf{K}^{\mathscr{K}}$, $\boldsymbol{\theta}^{\mathscr{K}}$ and $\mathbf{R}^{\mathscr{K}}_{equi}$
    Solve the system $\mathbf{K}^{\mathscr{K}}\mathbf{I}^{\mathscr{K}} = \mathbf{R}^{\mathscr{K}}_{equi}$
    Calculate $\tilde{\mathscr{E}}_{\mathscr{K}} = \|\tilde{\mathbf{e}}_p\|_{\mathscr{U}(\mathscr{K})}$
    $\|\tilde{\mathbf{e}}_p\|^2_{\mathscr{U}} = \|\tilde{\mathbf{e}}_p\|^2_{\mathscr{U}} + (\tilde{\mathscr{E}}_{\mathscr{K}})^2$
  end for
  $\|\tilde{\mathbf{e}}_p\|_{\mathscr{U}} = \sqrt{\|\tilde{\mathbf{e}}_p\|^2_{\mathscr{U}}}$
  $\tilde{\mathscr{E}}_{\%} = \|\tilde{\mathbf{e}}_p\|_{\mathscr{U}} / \|\mathbf{u}_p\|_{\mathscr{U}}$
  if $\tilde{\mathscr{E}}_{\%} \leqslant TOL_{\text{error}}$ **then**
    End the algorithm {*Convergence of the adaptive procedure*}
  else if $\tilde{\mathscr{E}}_{\%} > \text{TOL}_{\text{error}}$ **then**
    $n_\upsilon = 0$
    $i_{\text{end}} = 0$
    repeat
      for $\omega_j = 1$ to N **do**
        Calcula $\tilde{\mathscr{E}}_{\omega_j} = \sum_{\mathscr{K} \in \omega_j} V_{\mathscr{K}} \tilde{\mathscr{E}}_{\mathscr{K}} / V_{\omega_j}$
      end for
      $\tilde{\mathscr{E}}_{max} = \max(\tilde{\mathscr{E}}_{\omega_j}, \omega_j = 1, \ldots, N)$
      for $\omega_j = 1$ to N **do**
        if $\tilde{\mathscr{E}}_{\omega_j} \geqslant \upsilon \tilde{\mathscr{E}}_{max}$ **then**
          if $p_{\omega_j} < p_{max}$ **then**
            $p_{\omega_j} = p_{\omega_j} + i_p$ {*Enrichment of the cloud* ω_j}
            $n_\upsilon = 1$
          else
            $i_{\text{end}} = i_{\text{end}} + 1$
          end if
        end if
      end for
      if $i_{\text{end}} = N$ **then**
        Stop the analysis {TOL_{error} *cannot be reached*}
      else if $n_\upsilon = 0$ **then**
        update υ to 90% of its value υ
      end if
    until $n_\upsilon = 1$
  end if
end loop

Table III. Global effectivity indices of each adaptive solution step.

Step	NDF	$\tilde{\mathscr{E}}_{\%}$	$\mathscr{E}_{\%}$	η
1	70	9.101%	9.713%	0.937
2	114	4.946%	5.328%	0.928
3	210	1.950%	2.078%	0.939
4	286	0.974%	1.004%	0.970
5	418	0.227%	0.242%	0.936
6	614	0.050%	0.054%	0.925

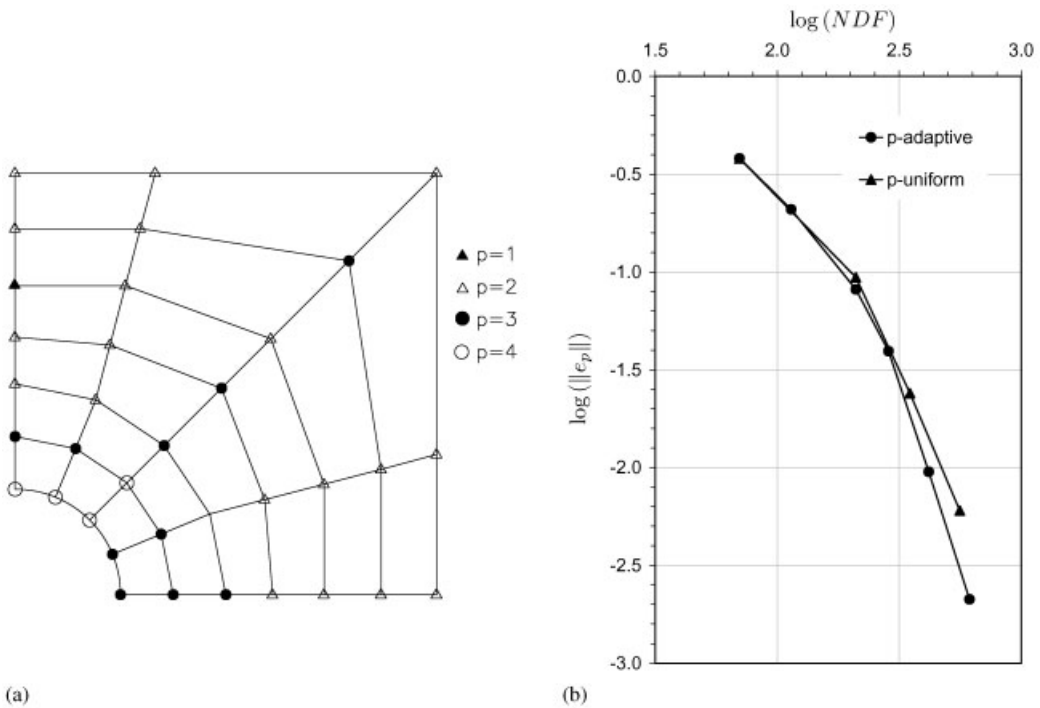

Figure 10. The performance of the p-adaptive refinement: (a) polynomial enrichment of the last adaptive step; and (b) convergence analysis.

to the ones employed in the conventional FEM with hierarchic shape functions for quadrilateral elements.

The aiming error tolerance ($\text{TOL}_{\text{error}}$) adopted in this example is 0.1%, i.e. $\tilde{\mathscr{E}}_{\%} \leqslant 0.1\%$. The convergence of the adaptive process is controlled by $\upsilon = 0.5$. In Table III the error estimator, the exact relative global error (using the energy norm of the exact global error and exact solution) and the global effectivity index (54) are presented for each adaptive step and the corresponding NDF which characterizes the approximation. At step 6, the adaptive procedure reaches convergence with $\tilde{\mathscr{E}}_{\%} = 0.1\%$. The resulting approximation presents the polynomial degree distribution depicted in the Figure 10(a). Aiming to evaluate the convergence rate of the adaptive analysis a comparative graphic is shown in the Figure 10(b), in which the logarithm of the error in energy norm is plotted versus the logarithm of the number of degrees of

freedom. In such graphic, the results of the p-adaptive analysis are plotted together with the convergence curve obtained with a sequence of uniform p-enrichment of the mesh represented in the Figure 8(b). It can be observed that an exponential rate of convergence is obtained for both of the refinement strategies. However, the use of the adaptive procedure gives, for this problem, slightly better results.

9. FINAL CONSIDERATIONS

The residual element method fits very well with the nodal enrichment strategy of the GFEM, not only due to the very direct way of building the approximation space $\mathscr{X}^0_{p+1}$ but also by considering the manner that the p-refinement is performed. By the numerical examples presented, the good quality of the adopted error measures was verified, then motivating their employment as a guide in a p-adaptive procedure. The suggested process, based on the equidistribution of error indicators associated with the nodes, is validated by a final example. However, a complete study of such procedure requires a processing time analysis or, even better, a floating point operations analysis. In spite of being a subject of future works, it is important to antecipate the information that the equilibrate procedure adopted here shall be improved for reducing the computational time which is eventually expensive without an equivalent compensation on the improvement of the numerical accuracy.

ACKNOWLEDGEMENTS

The authors gratefully acknowledge the Conselho Nacional de Desenvolvimento Científico e Tecnológico (CNPq) at Brazil for its joint support of this research project.

REFERENCES

1. Strouboulis T, Babuška I, Copps K. The design and analysis of the generalized finite element method. *Computer Methods in Applied Mechanics and Engineering* 2000; **181**(1–3):43–69.
2. Duarte CA, Babuška I, Oden JT. Generalized finite element methods for three-dimensional structural mechanics problems. *Computers and Structures* 2000; **77**(2):215–232.
3. Duarte CA, Oden JT. An h-p adaptive method using cloud. *Computer Methods in Applied Mechanics and Engineering* 1996; **139**:237–262.
4. Oden JT, Reddy JN. *An Introduction to the Mathematical Theory of Finite Elements*. Pure and Applied Mathematics. Wiley: New York, 1976.
5. Oden JT, Duarte CA, Zienkiewicz OC. A new cloud-based *hp* finite element method. *Technical Report*, *TICAM Report* 96-55, The University of Texas at Austin, Austin, Texas, USA, Dezembro 1996.
6. Oden JT, Demkowicz L, Rachowicz W, Westermann TA. Toward a universal h-p adaptive finite element strategy, part 2. A posteriori error estimation. *Computer Methods in Applied Mechanics and Engineering* 1989; **77**:113–180.
7. Ainsworth M, Oden JT. A posteriori error estimation in finite element analysis. *Computer Methods in Applied Mechanics and Engineering* 1997; **142**:1–88.
8. Ladevèze P, Maunder EAW. A general method for recovering equilibrating element tractions. *Computer Methods in Applied Mechanics and Engineering* 1996; **137**:111–151.
9. Babuška I, Caloz G, Osborn JE. Special finite element method for a class of second order elliptic problems with rough coefficients. *SIAM Journal on Numerical Analysis* 1994; **31**(4):745–981.
10. Melenk JM. On generalized finite element methods. *Ph.D. Thesis*, University of Maryland, College Park, 1995.
11. Melenk JM, Babuška I. The partition of unity finite element method: basic theory and applications. *Computer Methods in Applied Mechanics and Engineering* 1996; **39**:289–314.

12. Duarte CA, Oden JT. *Hp* clouds—a meshless method to solve boundary-value problem. *Technical Report*, *TICAM*, The University of Texas at Austin, May 1995.
13. Duarte CA, Oden JT. *H-p* clouds—an *h-p* meshless method. In *Numerical Methods for Partial Differential Equations*. Wiley: New York, 1996; 1–34.
14. Oden JT, Duarte CA, Zienkiewicz OC. A new cloud-based *hp* finite element method. *Computer Methods in Applied Mechanics and Engineering* 1998; **153**:117–126.
15. Belytschko T, Black T. Elastic crack growth in finite elements with minimal remeshing. *International Journal for Numerical Methods in Engineering* 1999; **45**:601–620.
16. Moës N, Dolbow J, Belytschko T. A finite element method for crack growth without remeshing. *International Journal for Numerical Methods in Engineering* 1999; **46**:131–150.
17. Strouboulis T, Copps K, Babuška I. The generalized finite element method. *Computer Methods in Applied Mechanics and Engineering* 2001; **190**:4081–4193.
18. Szabó B, Babuška I. *Finite Element Analysis*. Wiley: New York, 1991.
19. Chessa J, Wang H, Belytschko T. On the construction of blending elements for local partition of unity enriched finite elements. *International Journal for Numerical Methods in Engineering* 2003; **57**:1015–1038.
20. Oden JT, Duarte CA. Clouds, cracks and FEM's. In *Recent Developments in Computational and Applied Mechanics*, Reddy BD (ed.). International Center for Numerical Methods in Engineering, CIMNE: Barcelona, Spain, 1997; 302–321.
21. Duarte CA, Hamzeh ON, Liszka TJ, Tworzydlo WW. A generalized finite element method for the simulation of three-dimensional dynamic crack propagation. *Computer Methods in Applied Mechanics and Engineering* 2001; **190**:2227–2262.
22. Strouboulis T, Zhang L, Babuška I. Generalized finite element method using mesh-based handbooks: application to problems in domains with many voids. *SIAM Journal on Numerical Analysis* 1994; **31**(4): 745–981.
23. Stolarska M, Chopp DL, MOẼS N, Belytschko T. Modelling crack growth by level sets in extended finite element method. *International Journal for Numerical Methods in Engineering* 2001; **51**:943–960.
24. Demkowicz L, Oden JT, Strouboulis T. Adaptive finite elements for flow problems with moving boundaries. Part 1: variational principles and a posteriori error estimates. *Computer Methods in Applied Mechanics and Engineering* 1984; **46**:217–251.
25. Bank RE, Weiser A. Some a posteriori error estimators for elliptic partial differential equations. *Mathematics of Computation* 1985; **44**:283–301.
26. Babuška I, Rheinboldt WC. Error estimates for adaptive finite element method computations. *SIAM Journal on Numerical Analysis* 1978; **15**:736–754.
27. Babuška I, Rheinboldt WC. Adaptive approaches and reliability estimations in finite element analysis. *Computer Methods in Applied Mechanics and Engineering* 1979; **17/18**:519–540.
28. Babuška I, Strouboulis T, Upadhyay CS, Gangaraj SK, Copps K. Validation of a-posteriori error estimators by numerical approach. *International Journal for Numerical Methods in Engineering* 1994; **37**:1073–1123.
29. Babuška I, Strouboulis T, Upadhyay CS, Gangaraj SK. A model study of the quality of a posteriori estimators of linear elliptic problems. Part Ia: error estimation in the interior of patchwise uniform grids of triangles. *Computer Methods in Applied Mechanics and Engineering* 1994; **114**:307–378.
30. Duarte CA. A study of the p-version finite elements for elasticity and potential problems. *Master's Thesis*, Department of Mechanical Engineering, Federal University of Santa Catarina, Florianópolis, SC, Brazil, 1991 (in Portuguese).
31. Ohtsubo H, Kitamura M. Element by element a posteriori error estimation and improvement of stress solutions for two-dimensional elastic problems. *International Journal for Numerical Methods in Engineering* 1990; **29**:223–244.
32. Ohtsubo H, Kitamura M. Element by element a posteriori error estimation of the finite element analysis for three-dimensional elastic problems. *International Journal for Numerical Methods in Engineering* 1992; **33**:1755–1769.
33. Barros FB. Meshless methods and generalized finite element method in structural nonlinear analysis. *Ph.D. Dissertation*, São Carlos Scholl of Engineering, University of São Paulo, São Carlos, SP, Brazil, March 2002 (in Portuguese).
34. Timoshenko SP, Goodier JN. *Theory of Elasticity*. McGraw-Hill: New York, 1951.
35. Gordon WJ, Hall CA. Construction of curvilinear co-ordinate systems and applications to mesh generation. *International Journal for Numerical Methods in Engineering* 1973; **7**:461–477.

